Environmental Pollution xxx (2016) 1–9

Contents lists available at ScienceDirect

Environmental Pollution

journal homepage: www.elsevier.com/locate/envpol

High-resolution imaging of labile phosphorus and its relationship with iron redox state in lake sediments

Yulu Gao [a, b, d], Tao Liang [a, b, d, *], Shuhan Tian [a, b, d], Lingqing Wang [a, b], Peter E. Holm [c, d], Hans Christian Bruun Hansen [c, d]

[a] Key Laboratory of Land Surface Pattern and Simulation, Institute of Geographic Sciences and Natural Resources Research, Chinese Academy of Sciences, Beijing, 100101, China
[b] University of Chinese Academy of Sciences, Beijing 100049, China
[c] Department of Plant and Environmental Sciences, University of Copenhagen, Thorvaldsensvej 40, DK-1871, Frederiksberg C, Denmark
[d] Sino-Danish Center for Education and Research, Denmark

ARTICLE INFO

Article history:
Received 28 January 2016
Received in revised form
19 May 2016
Accepted 19 May 2016
Available online xxx

Keywords:
Phosphorus
Iron
DGT
High resolution
Sediment-water interface

ABSTRACT

A thorough understanding of the labile status and dynamics of phosphorus (P) and iron (Fe) across the sediment-water interface (SWI) is essential for managing internal P release in eutrophic lakes. Fe-coupled inactivation of P in sediments is an important factor which affects internal P release in freshwater lakes. In this study, two *in-situ* high-resolution diffusive gradients in thin films (DGT) techniques, Zr-Oxide DGT and ZrO-Chelex DGT, were used to investigate the release characteristics of P from sediments in a large freshwater lake (Dongting Lake, China; area of 2691 km^2) experiencing a regional summer algal bloom. Two-dimensional distributions of labile P in sediments were imaged with the Zr-Oxide DGT without destruction of the original structure of the sediment layer at four sites of the lake. The concentration of DGT-labile P in the sediments, ranging from 0.007 to 0.206 mg L^{-1}, was highly heterogeneous across the profiles. The values of apparent diffusion flux (F_d) and release flux (F_r) of P varied between −0.027–0.197 mg m^{-2} d^{-1} and 0.037–0.332 mg m^{-2} d^{-1}, respectively. Labile P showed a high and positive correlation ($p < 0.01$) with labile Fe(II) in the profiles, providing high-resolution evidence for the key role of Fe-redox cycling in labile P variation in sediments.

1. Introduction

Accumulation and leaching of phosphorus (P) has been widely studied in recent decades. Excess release of P from anthropogenic activities has led to widespread eutrophication and algal blooms in receiving water bodies (Kraal et al., 2015; Schindler, 2006). Once P from either diffuse or point sources enters freshwater systems, it may accumulate in sediments by deposition, adsorption or biological absorption, resulting in high internal P loads (Correll, 1998; Hupfer et al., 2007). Sediments are able to sorb or release P and act as a sink or source of water column nutrients (Boström et al., 1988; Smith and Schindler, 2009; Tang et al., 2014). Even if the sources of external P loading are removed or reduced, the water quality may not recover due to release of P accumulated in the sediments (Liu et al., 2016; Søndergaard et al., 2003; Pitkänen et al., 2001; Knuuttila et al., 1994).

In aquatic systems, P bound to amorphous iron (Fe) (oxyhdr) oxides is considered as one of the most active inorganic P pools, although apatite or $CaCO_3$ bound P is also important (Golterman, 1977; Golterman, 1988, 1995; Søndergaard et al., 2003). Under anoxic or anaerobic conditions, the reductive dissolution of iron (oxyhydr)oxides may be one of the main mechanisms responsible for sediment P release (Murray and Hesterberg, 2006). This P-Fe coupling model was first proposed by Einsele (1936) and later supported by many other studies (Mortimer, 1941; Petticrew and Arocena, 2001). Strong correlation between hypolimnetic Fe and P has been observed (Amirbahman et al., 2003). High P release flux was observed when the upward flux of Fe(II) was restricted by the precipitation of iron sulfide coupled with sulphate reduction (Jensen et al., 1995). Iron(III) reducing bacteria can transfer electrons from organic matter to iron (oxyhydr)oxides, causing the release of Fe(II) and P (Watts, 2000). However, other processes also cause the release of sediment P. Mineralization of organic matter

* Corresponding author. Room 3722, 11A, Datun Road, Chaoyang District, Beijing 100101, China.
E-mail address: liangt@igsnrr.ac.cn (T. Liang).

http://dx.doi.org/10.1016/j.envpol.2016.05.053
0269-7491/

(containing P) may cause the release of P (Golterman, 2001), and this release can be accelerated by bioturbation including enhanced microbial and chemical breakdown (Hansen et al., 1997). Phosphate may sorb onto aluminum (hydr)oxides (Monbet et al., 2008) and also it may precipitate with as calcium phosphates (House et al., 1986). The decreased pH with depth due to the CO_2 production by mineralization can lead to the dissolution of $CaCO_3$ as well as release of calcium phosphates (Mayer et al., 1999). The release of P may also be increased due to resuspension and this increase can be mitigated by macrophytes (Søndergaard et al., 1992; Wu and Hua, 2014). Macrophytes can pump P from sediments during the growing season (Stephen et al., 1997) and the plant litter can act as organic P sources. As many complex interactions may affect the examination of Fe-P coupling, a more direct proof is required.

Incubation of intact sediment cores has been commonly used to observe the sediment-water interface (SWI) process and estimate the flux across the SWI (Schoepfer et al., 2015; Funes et al., 2016). For estimating the P and Fe lability in sediments, previous studies mostly used *ex-situ* chemical extraction methods to determine the concentration of loosely-sorbed P and redox-sensitive P bound to iron (oxyhydr)oxides (Psenner and Pucsko, 1988; Penn et al., 1995; Rydin, 2000; Reitzel et al., 2005; Hupfer et al., 2009). Measurement of labile P and Fe status by *ex-situ* chemical extraction procedures can estimate the total amount of labile P that existed in the sediments at the time of sampling, but cannot fully characterize its dynamics. Analytical errors due to destruction of the original structure of the sediment layer and exposure of sediment samples to the air can also occur. The sediments in lakes, especially the zones close to SWI, are generally highly heterogeneous and sensitive to physical and biological disturbances. High-resolution measurements will allow for evaluation of more precise concentration gradients across SWI.

The diffusive gradients in thin films (DGT) technique is an *in-situ* technique based on the Fick's First Law, which can account for labile fractions in pore water as well as additional labile P that can readily release from the sediment solids and resupply to the pore water concentration (Zhang and Davison, 1995). These features of DGT allow for collection of data characterising the dynamics of the target solutes and to help minimizing the analytical errors caused by conventional chemical extraction methods (Zhang et al., 2014; Panther et al., 2011; Pichette et al., 2009; Monbet et al., 2008). Recently, a new technique (Zr-oxide DGT) was developed to allow for two-dimensional (2D) imaging of labile P in sediments at a submillimeter resolution (Ding et al., 2013). A second DGT technique (ZrO-Chelex DGT), was developed for simultaneous measurement of labile P and labile Fe in sediments at a millimeter resolution (Xu et al., 2013). This new DGT technique provides advantages for estimation of labile P and Fe at high resolution as well as their relationships.

This current study seeks to advance the understanding of labile P, as well as Fe and P dynamics, in the sediments of freshwater lakes. The two-dimensional distribution of labile P at SWI was imaged at submillimeter resolution using Zr-Oxide DGT. The relationship between labile P and labile Fe(II) in the profiles was analyzed based on the simultaneous measurement with the ZrO-Chelex DGT. Furthermore, Fick's law and data from intact sediment core incubation experiments were used to calculate the fluxes across SWI and to determine whether sediment acted as a sink or source for P at each sampling site.

2. Materials and methods

2.1. Study area and sampling sites

Dongting Lake (111°40′–113°10′E, 28°38′–29°45′N) is the second largest freshwater lake in China comprising of a series lakes and three major regions denoted East, South, and West Dongting Lakes (Fig. 1). The entire lake has a surface area of 2691 km^2 with a mean depth of 6.39 m. Large amounts of phosphorus has been introduced to Dongting Lake and hence eutrophication and high P concentrations have been previously measured (Wang et al., 2014).

Samples were collected in January 2015 and *in-situ* water parameters including temperature, pH and Dissolved Oxygen (DO) were measured using an *in-situ* water quality analyzer (HORIBA, U-53). Three sediment cores (84 mm in diameter, 15 cm and 25 cm in length for overlying water and sediment, respectively) for each site were collected. Four sites denoted WD, SD, ED and LJ were selected from the typical regions of West, South, East Dongting Lake, and a crucial cross-section between South and East Dongting Lake, respectively. As the whole Dongting Lake system is composed of a series of big lakes, this study mainly focused on the four typical regions instead of covering the whole lake system. Among these sites, WD is primarily influenced by agricultural contaminants and experiences algal blooms during summer months. SD is located in a region with relatively low levels of nutrient contamination (Wang et al., 2014). ED is close to Yueyang City and it is affected by domestic and industrial wastewater discharges. Several villages are distributed around LJ and its water quality is often influenced by livestock and poultry breeding and untreated domestic sewage.

2.2. Preparation and deployment of DGT probes

DGT probes equipped with Zr-oxide gel as a binding layer were used to obtain two-dimensional distribution of labile P in sediments at a submillimeter resolution. The DGT probes equipped with ZrO-Chelex gel as a binding layer were used for simultaneous measurements of labile P and labile Fe in sediments at a millimeter resolution in the vertical direction. The details of the two preparation procedures for preparation of Zr-oxide and ZrO-Chelex gels have been described previously by Ding et al. (2011) and Xu et al. (2013). The diffusive gel was prepared with 15% acrylamide and 0.3% agarose-derived cross-linker based on the method of Scally et al. (2006). Flat probes with dimensions of 18 × 160 mm (width × length) exposure area were used for measurements. During the set-up for both types of DGT, the binding gel (with the binding agent surface facing up) was covered sequentially by a 0.4-mm-thick diffusive gel and a 0.13-mm-thick cellulose nitrate filter membrane (0.45-μm pore size, Whatman, UK). The Zr-oxide DGT and ZrO-Chelex DGT probes were deoxygenated with nitrogen for at least 16 h and kept in the oxygen-free water prior to deployment in the sediments. The ZrO-Chelex DGT probes were deployed into the sediments simultaneously with Zr-oxide DGT probes and removed after 24 h. Experiments were conducted in triplicate for each site.

2.3. Phosphorus flux simulation experiment based on incubation of intact sediment cores

Phosphorus flux experiments across the SWI based on incubation of the intact sediment cores were performed according to the methods of Zhang et al. (2006). The overlying water level was maintained 15 cm above the SWI and the sediments were maintained 25 cm below the SWI without disturbing the inner structure (Boers and Hese, 1988; Fan et al., 2002). Polyvinyl chloride tubes (84 mm in diameter, 50 cm in length) filled with 40-cm-height *in-situ* water without sediment were used as the control. All tubes were placed in a constant temperature (equivalent to the sampling temperature) incubator in the dark. A two milliliter water sample was collected 5 cm above the interface by pipetting gently so as not to disturb the SWI. The water was sampled at 0, 0.25, 0.5, 1, 1.5, 2,

Please cite this article in press as: Gao, Y., et al., High-resolution imaging of labile phosphorus and its relationship with iron redox state in lake sediments, Environmental Pollution (2016), http://dx.doi.org/10.1016/j.envpol.2016.05.053

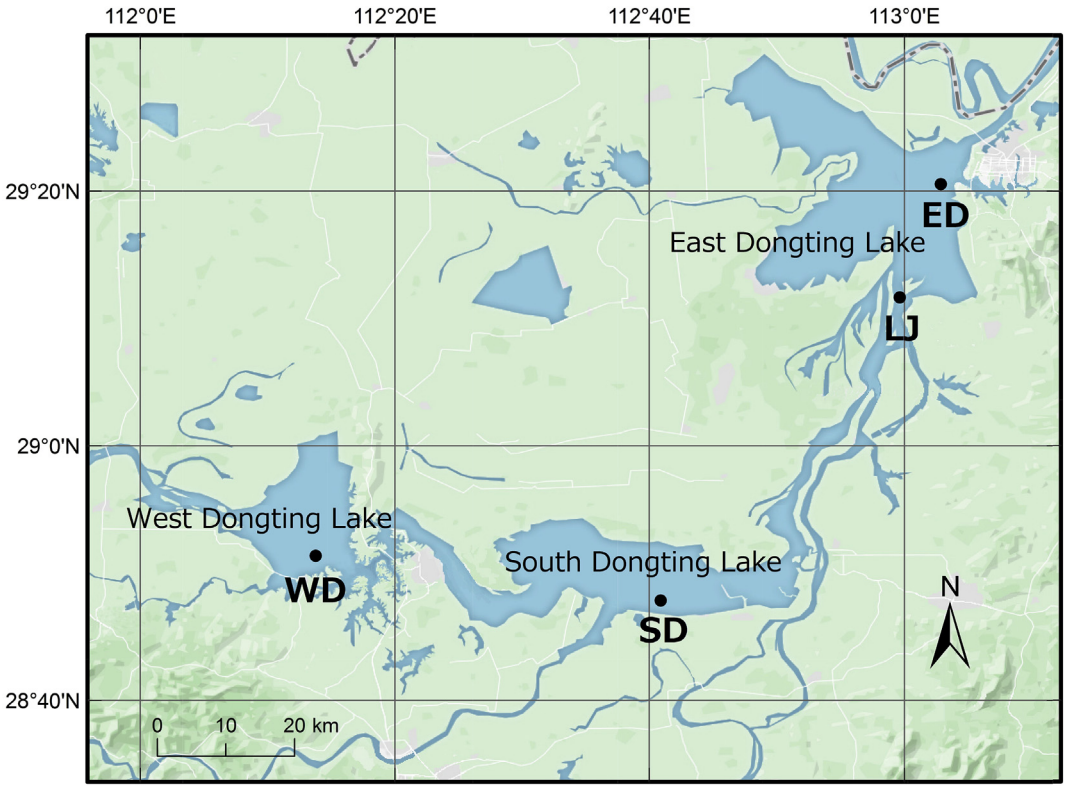

Fig. 1. Map of the Dongting Lake and sampling sites. The base map was image-captured with the software Mapbox.

and 3 days before deployment of DGT probes. After each sampling event, *in-situ* freshwater was added to the tubes gently and immediately.

2.4. Chemical analysis

After retrieval of the DGT probes, a 20-mm binding gel above the SWI and 120-mm binding gel below the SWI were used for analysis. The accumulated P in the Zr-oxide binding gels was colored by the conventional molybdenum blue method (Murphy and Riley, 1962) and measured by computer-imaging densitometry (5600F, Canon, Japan) according to the grayscale intensity on the gel surface. The detailed procedure and various parameters have been described previously by Ding et al. (2013). The retrieved ZrO-Chelex DGT was analyzed following the procedure of Xu et al. (2013) and the ZrO-Chelex binding gel was sliced at 1-mm intervals. Each gel slice was sequentially eluted in 0.4 mL of 1 M HNO_3 and 0.4 mL of 1 M NaOH solutions for 16 h and analyzed for labile Fe and P using a miniaturized spectrophotometry method (Epoch Microplate Spectrophotometer, Biotek, USA) as described by Xu et al. (2012).

Total P (TP) and dissolved reactive P (DRP) in water samples as well as DRP in DGT elutes were measured using the molybdenum blue method (Murphy and Riley, 1962). Concentrations of Fe(II) in the DGT elutes were determined using the phenanthroline colorimetric method (Tamura et al., 1974). COD was measured by a dichromate reflux method (Jin and Tu, 1990) and the redox potential of sediments was measured using a redox electrode (PHS-3E, Leici, China). Concentration of suspended solids (SS) was measured by filtration (0.45-μm pore size, Whatman, UK) according to the standard method (Jin and Tu, 1990).

The porosity of surface sediment was calculated from the bulk density and particle density. The particle density used the empirical value (2.65 mg m^{-3}) and the bulk density was measured by the cutting-ring method (Jin and Tu, 1990). Sediment cores were cut into 1-cm layers and the top 5-cm layers of sediment were used for chemical analysis. Sediment was freeze-dried and ground into particles able to pass through a 100-mesh nylon sieve. The pH was measured in a suspension (with 1:10 solid to liquid ratio) using a pH electrode (PB-10, Sartorius, Germany). The organic matter content in the sediments was estimated by TOC using a TOC analyzer (Vario TOC Cube, Elementar, Germany). To partition P in the sediments, a modified chemical sequential extraction method following Rydin (2000) was used. Loosely sorbed P (LS-P), redox sensitive P (Fe-P), aluminum-bound P (Al-P), organic P (Org-P), carbonate and apatite P (Ca-P), and Residual P (Res-P) were determined by following the procedure outlined in Supplementary Table S1. Phosphorus in the different fractions was determined by the molybdenum blue/ascorbic acid method (Rodriguez et al., 1994) and Res-P was taken as the difference between TP and all other P fractions. Sediment samples were digested with HNO_3—HF—$HClO_4$ to determine total P, Fe, Al and Ca (Liang et al., 2005; Wang et al., 2011). Concentrations of P, Fe, Al and Ca in the digested solutions were measured using inductively-coupled plasma-optical emission spectrometry (ICP-OES, OPTIMA 5300DV, Perkin Elmer, USA). The accuracy of the analysis was checked using standard reference material for lake sediments (GBW07436, Center for Standard Reference of China).

2.5. Data processing

Concentrations of labile P and labile Fe(II) as measured by DGT (C_{DGT}) were calculated by Eq. (1):

$$C_{DGT} = \frac{M\Delta g}{DAt} \quad (1)$$

Please cite this article in press as: Gao, Y., et al., High-resolution imaging of labile phosphorus and its relationship with iron redox state in lake sediments, Environmental Pollution (2016), http://dx.doi.org/10.1016/j.envpol.2016.05.053

where Δg is the thickness of the diffusive layer, D is the diffusion coefficient of the phosphate or Fe(II) in the diffusive layer at experimental temperature (12 °C), t is the deployment time (24 h), A is the exposed area of the gel, and M is the measured accumulated mass of P or Fe(II) (Xu et al., 2013; Zhang and Davison, 1995; Ding et al., 2013).

The apparent diffusion flux (F_d) of P across the SWI was quantified from the DGT-labile P profiles using Fick's First Law according to Eq. (2) (Ding et al., 2015). Considering the different resupplying mechanisms of DGT measurement from overlying water and sediments, the apparent diffusion flux across the SWI was estimated as the sum of diffusion fluxes from overlying water to the SWI and from the sediment to the SWI.

$$F_d = J_W + J_S = -D_W\left(\frac{\delta C_{DGT}}{\delta x_w}\right)_{(x=0)} - \phi D_S\left(\frac{\delta C_{DGT}}{\delta x_s}\right)_{(x=0)} \quad (2)$$

where J_w and J_s are the flux of P from the overlying water to the SWI and from the sediment to the SWI, respectively; D_w and D_s are the diffusion coefficients of HPO_4^{2-} in water and sediments, respectively; $\left(\frac{\delta C_{DGT}}{\delta x_w}\right)_{(x=0)}$ and $\left(\frac{\delta C_{DGT}}{\delta x_s}\right)_{(x=0)}$ are the DGT-labile concentration gradients in the overlying water and sediments, respectively. In order to achieve an accurate estimation of the flux, one-dimensional distributions of labile P measured by Zr-oxide DGT with submillimeter resolution were used for estimating the gradients. The average concentrations of DGT-labile P from the 5 mm depth in the water above the SWI to 5 mm in the sediment below the SWI were used to obtain the one-dimensional distributions. An exponential function was applied for the fitting (Spagnoli and Bergamini, 1997). The diffusion coefficient in sediments (D_s) was estimated using Eq. (3) (Ullman and Aller, 1982).

$$D_S = \frac{D_w}{\phi F} \quad (3)$$

where ϕ is the porosity in sediment, F is the formation resistivity factor, and D_w is the diffusion coefficient of HPO_4^{2-} in water calibrated by the actual temperature (Li and Gregory, 1974). The porosity ϕ was used to determine the formation resistivity factor F with $F = \frac{1}{\phi^3}$ for $\phi \geq 0.7$ and with $F = \frac{1}{\phi^2}$ for $\phi < 0.7$, respectively (Manheim and Waterman, 1974).

The release flux (F_r) based on incubation of intact sediment cores was calculated using Eq. (4) according to Zhang et al. (2006).

$$F_r = \left[V(c_n - c_o) + \sum_{j-1}^{n} V_{j-1}(c_{j-1} - c_a)\right] \Big/ (S \cdot t) \quad (4)$$

where V is the volume of the overlying water in the tube; c_0 is the concentration of phosphate in the overlying water before sampling; c_n and c_{j-1} are the concentrations of phosphate in the water samples at the n time and the (j-1) time of sampling, respectively; c_a is the concentration of phosphate in the *in-situ* water added into the tube; V_{j-1} is the volume of water sample sampled at the (j-1) time; S is the contact area of the sediment-water interface; t is the experimental time.

SPSS 19.0 was used to provide a quantitative explanation (Spearman's rank correlation) of the relationship between labile P and labile Fe(II) at millimeter resolution. The correlations between phosphate concentration in overlying water and incubation period were analyzed using linear fitting with the least squares approach.

3. Results and discussion

3.1. Basic physicochemical properties of overlying water and sediments

The physicochemical properties of overlying water and sediments at each site are shown in Tables 1 and 2, respectively. The total P and DRP in the overlying water ranged between 0.039 and 0.088 mg L^{-1} and 0.010–0.036 mg L^{-1}, respectively. The total P in sediments varied from 0.52 to 0.89 mg g^{-1}. Higher values of TP and DRP and greater contributions of DRP to TP in the overlying water were observed at the sites with higher TP contents in sediments (WD and LJ). The pH values of the sediments of WD (~6.62) and LJ (~6.71) were lower than those of SD (~7.21) and ED (~7.25). The sediment TOC content was low at SD (8.99 mg g^{-1}) but relatively high (16.6–25.6 mg g^{-1}) at the other three sites, which were highly influenced by agricultural emissions and domestic sewage. The contents of total Fe and Al in the sediments ranged from 33.3 to 48.1 mg g^{-1} and 56.4–76.6 mg g^{-1}, respectively. The total Ca content in sediments was relatively low (1.69–5.59 mg g^{-1}), especially at SD.

3.2. Sediment P pool

The different fractions of P extracted sequentially from the top 5-cm sediment layer are shown in Table 2. LS-P (0.0007–0.006 mg g^{-1}) was the largest bioavailable and loosely bound fraction of P, but only accounted for less than 1% of TP content. Fe-P, which varied between 0.06 and 0.13 mg g^{-1}, represented the redox-sensitive P bound to iron and manganese (oxyhydr)oxides (Rydin, 2000). This fraction contributed 9.6–14.9% of TP. Although the Fe-P pool was not the largest of the sediment P pools, Fe-P is still considered an important bioavailable P pool due to its high activity (Li and Huang, 2010). Al-P (0.17–0.35 mg g^{-1}), which is the fraction of P mainly bound to Al (oxyhydr)oxides (exchangeable with OH^-), occupied a large fraction of TP, ranging from 25.0% to 48.1%. Org-P (0.02–0.05 mg g^{-1}) contributed to 2.3–7% of TP, suggesting that organic P bound in humic compounds and P in microorganisms including poly-P and detritus in the sediments remained at low levels. Both Ca-P (0.01–0.08 mg g^{-1}) and Res-P (0.18–0.44 mg g^{-1}) are regarded as non-bioavailable fractions in the sediment, with Res-P as the most abundant P fraction (24.5%–51.2% of TP) at most sites investigated. For the mobile P fractions, the highest LS-P values and its greatest contributions to TP were observed at site WD. The contents of Fe-P were almost two times higher at sites WD and LJ than those at sites ED and SD. However, the sorption capacity of Al and Fe oxides is not known as their identity, crystallinity and specific surface area is not known (Jan et al., 2013). Additionally, the actual environmental conditions, such as redox potential, would greatly influence the true P lability in sediments. Thus, more direct evidence to reflect the labile status of P and the adsorption characteristics of the sediments would be preferred.

3.3. High-resolution imaging of DGT-labile P in profiles

The two-dimensional imaging data of labile P are shown in Fig. 2. High heterogeneity in the distribution of labile P across profiles can be observed. The labile P measured by DGT in the overlying water varied from 0.007 to 0.042 mg L^{-1}. The order of the four sites based on mean concentration of labile P in overlying water was WD > LJ > ED > SD. This result was consistent with the DRP concentrations measured in water samples. In sediments, the concentration of labile P ranged between 0.012–0.206 mg L^{-1}, 0.007–0.045 mg L^{-1}, 0.010–0.177 mg L^{-1} and 0.007–0.051 mg L^{-1}

Please cite this article in press as: Gao, Y., et al., High-resolution imaging of labile phosphorus and its relationship with iron redox state in lake sediments, Environmental Pollution (2016), http://dx.doi.org/10.1016/j.envpol.2016.05.053

Table 1
Physicochemical properties of overlying water samples collected in Dongting Lake.

Sampling site	WD	SD	LJ	ED
Temperature (°C)	12.1	11.7	12.0	11.8
pH	7.5	7.9	7.6	7.5
DO (mg L^{-1})	9.98	9.37	9.63	9.45
COD (mg L^{-1})	1.44	1.12	1.92	1.24
SS (mg L^{-1})	5	4	30	129
Total P (mg L^{-1})	0.077	0.039	0.088	0.053
DRP (mg L^{-1})	0.036	0.010	0.029	0.012
Proportion of DRP in TP (%)	47	26	33	23

for WD, SD, LJ and ED, respectively. Generally, higher values of labile P were found with increasing depth in the sediments. The concentrations of labile P in the sediments at sites WD and LJ were higher than those at sites SD and ED. A previous study showed that DGT-labile P concentrations in sediments were higher at the algal-dominated regions (0.12–0.35 mg L^{-1} at the 50–120 mm depth below the SWI) when compared with central regions or macrophyte-dominated regions (Ding et al., 2015). And the bioavailable P was reported to be highly correlated ($R^2 = 0.941$, $p < 0.01$) with DGT-labile P (Xu et al., 2011). Thus, the sites with higher labile P concentrations, such as WD and LJ, are likely at greater risk of algal bloom. As the distributions of P can be reflected at the submillimeter high-resolution, some small spots, with less than 4 mm diameter and enhanced concentrations of labile P (~0.206 mg L^{-1}), was seen in profiles of WD. A concentrated spot (~0.051 mg L^{-1}) with 7 mm diameter can also be seen in the sediments of ED. These spots have been reported previously in other lakes (Ding et al., 2012), and have been attributed to decomposition of organic matter (Widerlund and Davison, 2007).

3.4. Estimation of P flux in two different ways

The values of the apparent diffusion flux (F_d) reflected P diffusion across SWI based on Fick's First Law. The sediments at sites with positive F_d (WD, LJ and ED) acted as sources of P (Fig. 3). In contrast, the sediments of SD with negative F_d (-0.027 mg m^{-2} d^{-1}) tended to take in P from the overlying water. The F_d in WD (0.197 mg m^{-2} d^{-1}) and LJ (0.088 mg m^{-2} d^{-1}) was high, and approximately consistent with F_d measured in algal-dominated bays with high internal loading of P of a large eutrophic lake (Lake Taihu, China, with an area of 2338 km^2) (Ding et al., 2015). Regions with high content of P in sediments are particularly important, as porewater in the sediments may have similar physicochemical properties with those of the overlying water under anaerobic conditions. Under these conditions, the resistance during the concentration-gradient diffusion process is reduced, and the potential for P release from sediments to water column is enhanced. The F_d of P was calculated based on the labile P concentration gradients measured by Zr-oxide DGT within ±5 mm distance to the SWI. Parameters in the calculation are shown in Table 3. As the high-resolution concentration data were used and high correlation coefficients (R^2) for the exponential curve fitting were obtained (except for the overlying water at ED) (Supplementary Figs. S1 and S2), the error in the concentration gradients were small. The correlation coefficient (R^2) for the overlying water at ED (0.64) was much lower than at other sites, which might be due to the high SS concentrations (Table 1). The stable concentration gradient may not form in the overlying water due to random movement of large amount of SS, indicating that the F_d is not an accurate estimation for the sites with high SS concentrations.

The values of release flux (F_r) of P, which were calculated from incubation of intact sediment cores, varied between 0.037 and 0.332 mg m^{-2} d^{-1} (Fig. 3). High internal P loading rates were observed at WD (0.332 mg m^{-2} d^{-1}) and LJ (0.234 mg m^{-2} d^{-1}). These two sites also had high F_d of P as well as high labile P contents in the sediments. A positive linear correlation ($p < 0.05$) between phosphate concentration in the overlying water and duration of the incubation period was found for each site (Supplementary Fig. S3). The linear correlation coefficient at site ED (0.78) was lower than at other sites, indicating that the incubation method may also not be suitable for estimating the flux at sites with high SS concentrations. Based on the data from incubation experiment, the sediments at SD tended to release P to overlying water, which was not consistent with the result of F_d. Additionally, the values of F_r were higher than F_d for each of the four sites. Therefore, the apparent diffusion flux was underestimated and may not reflect the actual fluxes. Furthermore, the resupply of P to porewater and the resulting diffusion does not represent the total flux across the SWI. Other factors such as uptake of P by macrophytes (Stephen et al., 1997), hydrodynamics (You et al., 2007) and bioturbation (Chen et al., 2015) may also contribute to the flux variation of P. However, there was no evidence of obvious accelerated P cycling caused by uptake of P into macrophytes, as reported in the macrophyte-dominated regions of Lake Taihu with high flux of P but low concentrations of P in overlying water (Ding et al., 2015; Zhang et al., 2006). These differences may be due to the lack of adequate growth conditions for macrophytes at the sampling sites in winter (mainly low temperatures).

The average values of F_r/F_d for WD, SD, LJ and ED were 1.69, −1.37, 2.66, and 5.50, respectively (Fig. 3). To some extent, the F_r/F_d ratio describes the abundance of benthos and benthic activity (Cermelj et al., 1997; McCall and Tevesz, 1982). At the site (ED) with high SS concentration, the F_r/F_d ratio was not well estimated. The F_r/F_d ratio at LJ was higher than that at WD, suggesting more active bioturbation on P lability at LJ than WD.

3.5. Labile P release characteristics concerning P-Fe relationship

The distribution of labile P and labile Fe(II) in profiles are shown in Fig. 4. The concentrations of labile P in WD and LJ sediments were approximately 6–10 times higher than those in sediments of SD and ED, consistent with 2D imaging data. However, labile Fe(II) did not exhibit the same clear differences among sites as labile P

Table 2
Physicochemical properties of the top 5-cm layer of sediments collected in Dongting Lake.

Sampling site	pH	TOC (mg g^{-1} DW)	Total P (mg g^{-1} DW)	Total Fe (mg g^{-1} DW)	Total Al (mg g^{-1} DW)	Total Ca (mg g^{-1} DW)	Concentrations of different P fractions (mg g^{-1} DW)						Proportions of different P fractions in TP (%)					
							LS-P	Fe-P	Al-P	Org-P	Ca-P	Res-P	LS-P	Fe-P	Al-P	Org-P	Ca-P	Res-P
WD	6.62	17.5	0.89	44.9	76.7	3.15	0.006	0.13	0.27	0.03	0.06	0.39	0.7	14.9	29.9	3.2	7.2	44.1
SD	7.21	8.99	0.52	33.3	62.3	1.69	0.0007	0.06	0.17	0.03	0.01	0.24	0.1	12.0	33.3	5.4	1.9	47.3
LJ	6.71	16.6	0.86	48.1	56.4	5.59	0.001	0.10	0.21	0.02	0.08	0.44	0.1	11.9	25.0	2.3	9.5	51.2
ED	7.25	25.6	0.73	43.4	71.2	5.60	0.002	0.07	0.35	0.05	0.08	0.18	0.2	9.6	48.1	7.0	10.6	24.5

Please cite this article in press as: Gao, Y., et al., High-resolution imaging of labile phosphorus and its relationship with iron redox state in lake sediments, Environmental Pollution (2016), http://dx.doi.org/10.1016/j.envpol.2016.05.053

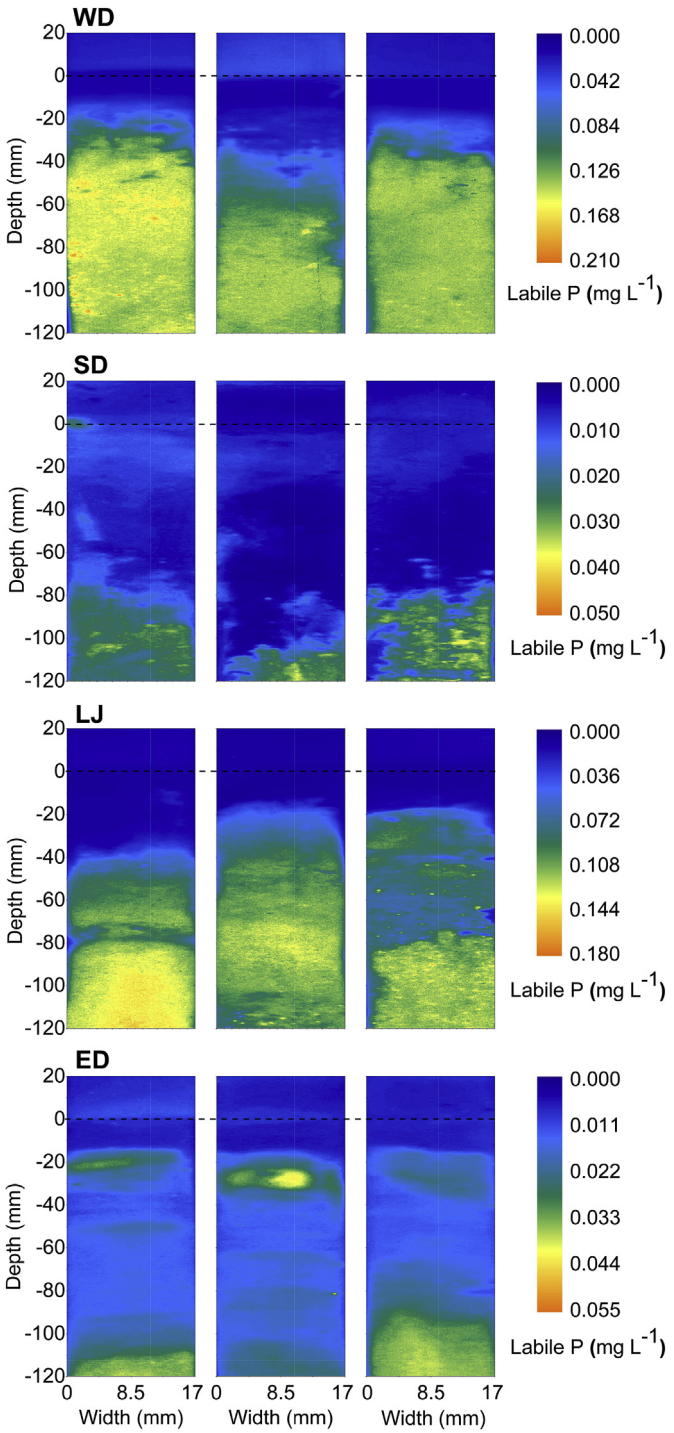

Fig. 2. Vertical distribution of labile P in profiles from 4 sites as determined by Zr-oxide DGT. Each site had 3 replicates. The sediment-water interfaces are shown by the dashed lines. The concentration of labile P in overlying water and sediments are shown above the dashed line and below the dashed line, respectively.

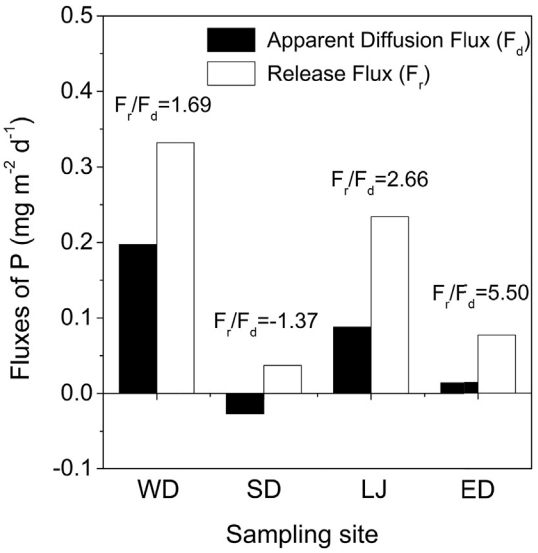

Fig. 3. Comparison between apparent diffusion fluxes (F_d) and release fluxes (F_r) of P.

did. As the redox potential was high in the top layer of sediments (Supplementary Fig. S4), the concentration of labile Fe(II) remained at a relatively low value (0.02–0.07 mg L^{-1}) in the surface sediments of the four sites. Below the oxidized surface sediments, the labile Fe(II) concentrations increased, followed by a slight decrease, and then the concentrations increased with depth again and became stable at a relatively high level in the deep sediment layers (90–120 mm).

The relationships between labile P and Fe(II) were examined through Spearman's rank correlation coefficients (Table 4). Statistically positive correlations ($p < 0.01$) between labile P and labile Fe(II) was found for each of the four sites. Iron redox cycling is presumably a key mechanism for controlling phosphate adsorption and desorption and hence for the control of labile P concentrations at the SWI. The high-resolution determination of labile P and Fe(II) profiles demonstrate that the iron redox control works even at millimeter scale, which has been verified in details in another shallow Lake Taihu, China (Ding et al., 2016). Thus, the decrease of labile Fe(II) in upper sediments may be attributed to oxidation of Fe(II) and the subsequent precipitation of Fe(III) (oxyhydr)oxides at relatively high redox potentials (Lewandowski and Hupfer, 2005). The newly precipitated Fe(III) (oxyhydr)oxides offers more adsorption sites for labile P, resulting in an increase in iron oxide-bound P and decrease in labile P (Lewandowski et al., 2007). The increase in labile P in the deeper sediments may be due to the reduction of Fe(III) to Fe(II) at lower redox potentials (Christophoridis and Fytianos, 2006), which can result in precipitation of ferrous phosphate or transfer of P to the sediment pore-water. However, other processes, such as precipitation with sulfide under reducing conditions (Olsen, 1964; Mejia et al., 2016; Roden and Zachara, 1996) and increased thickness of the oxygenated layer due to high concentration of nitrate (Jensen and Andersen, 1992), may also influence the Fe(II) profiles and hence the Fe controlled P solubility. Moreover, P mobility in sediments can also be enhanced by other processes such as mineralization of organic matters (Suzumura and Kamatani, 1995), apatite dissolution (House et al., 1986) and release of bacterial polyphosphates (Hupfer et al., 1995).

The ratio of labile Fe to labile P was calculated from the slope in the linear correlations (Fig. 5). Low values of the labile Fe(II)/P ratio were observed at sites WD and LJ (6.4 and 7.5, respectively), while high values were seen for sites SD and ED (48.5 and 41.7, respectively). The result reflects clear differences in adsorption ability of Fe(III) (oxyhydr)oxides to control P lability among sites. It is consistent with the result of P fluxes as well as the concentrations of labile P measured. Jensen et al. (1992) have suggested a critical value of 15 for the total Fe/P ratio to estimate whether there is sufficient adsorption capacity for aerobic surface sediments to

Please cite this article in press as: Gao, Y., et al., High-resolution imaging of labile phosphorus and its relationship with iron redox state in lake sediments, Environmental Pollution (2016), http://dx.doi.org/10.1016/j.envpol.2016.05.053

Table 3
Estimated parameters for calculation of apparent diffusion flux (F_d) of P across the sediment-water interface.

Sampling site	F_d of P from overlying water to SWI			F_d of P from sediments to SWI			
	Dw (10^{-6} cm^2 s^{-1})	R^2	$\left(\frac{\delta C_{DGT}}{\delta x_w}\right)_{(x=0)}$	ϕ	Ds (10^{-6} cm^2 s^{-1})	R^2	$\left(\frac{\delta C_{DGT}}{\delta x_s}\right)_{(x=0)}$
WD	5.0746	0.98	0.0036	0.71	2.5581	0.83	0.0025
SD	5.0746	0.94	−0.0008	0.59	2.9940	0.93	0.0005
LJ	5.0746	0.98	0.0019	0.81	3.3294	0.85	0.0002
ED	5.0746	0.65	−0.0004	0.92	4.2951	0.95	0.0009

R^2: The correlation coefficients of exponential curve fittings of the concentration gradients.

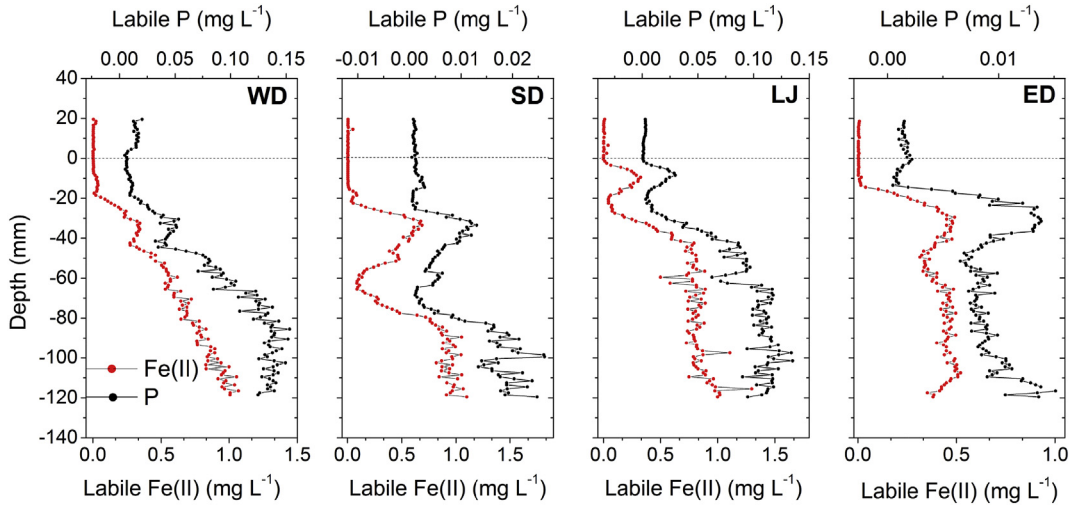

Fig. 4. One-dimensional changes of labile P and Fe(II) measured by ZrO-Chelex DGT in profiles. The sediment-water interfaces are shown by the dashed lines.

buffer phosphate concentrations and control the internal P release. The ratio of total Fe to total P in sediments of WD, SD, LJ and ED was 50.4, 64.1, 56.0 and 59.4, respectively. All of the ratios were higher than the critical value. However, the total Fe/P ratios only showed limited differences among the four sites and underestimated the differences in lability of the P as much more P is released per Fe(II) produced at sites WD and LJ compared with sites SD and ED. An Fe(II)/P ratio much lower than the total Fe/P ratio indicates that P rich Fe(III) (oxyhydr)oxides are preferentially reduced and dissolved. The reason may be that these are very small particles with a high specific surface area, and that the Fe(III) (oxyhydr)oxide particles being dissolved is mainly particles in recent deposits that contain much P. As the labile Fe(II) is much more relevant for the sediment P cycle, the labile Fe(II)/P ratio may provide more accurate assessment compared to the total Fe/P ratio for determining the Fe-coupled P release in sediments.

Table 4
Spearman's rank correlation coefficients between labile P and labile Fe(II) at different sampling sites.

Sampling site	WD	SD	LJ	ED
Spearman's rank correlation coefficients	0.928**	0.855**	0.889**	0.692**

**Correlation is significant at the 0.01 level (2-tailed).

4. Conclusions

The concentrations of DGT-labile P determined by two-dimensional imaging at a submillimeter resolution ranged from 0.007 to 0.206 mg L^{-1} and suggest a high level of heterogeneity in

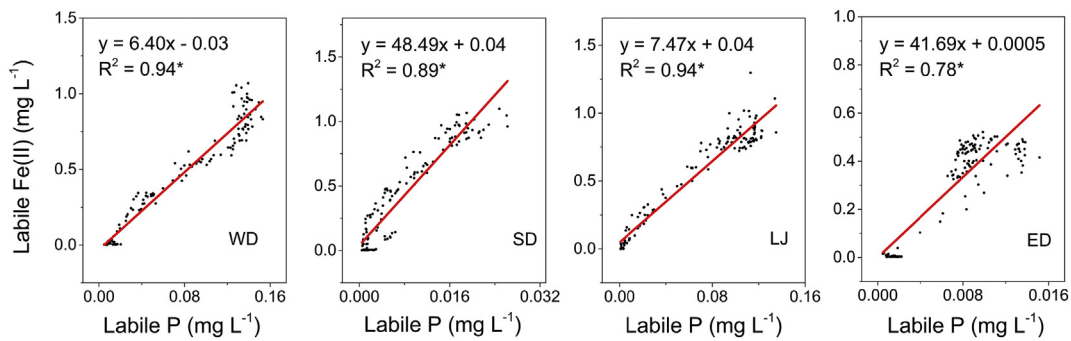

Fig. 5. Linear fitting between DGT-labile Fe(II) and DGT-labile P.

Please cite this article in press as: Gao, Y., et al., High-resolution imaging of labile phosphorus and its relationship with iron redox state in lake sediments, Environmental Pollution (2016), http://dx.doi.org/10.1016/j.envpol.2016.05.053

the lake sediments. The apparent diffusion flux of P across the SWI calculated based on the Fick's First Law and the release flux of P calculated from incubation of intact sediment cores varied between −0.027–0.197 mg m^{-2} d^{-1} and 0.037–0.332 mg m^{-2} d^{-1}, respectively. The concentrations and fluxes of labile P in the sediments of WD and LJ were higher than those of ED and SD. High and positive correlation ($p < 0.01$) between labile P and labile Fe(II) in profiles provided high-resolution evidence for the key role of Fe-redox cycling in labile P variation in sediments. The ratio of labile Fe(II) to labile P provided a more accurate assessment compared to the total Fe/P ratio for determining release of P when Fe(III) (oxyhydr) oxides are being reduced and hence for the iron-coupled P dynamics in sediments.

Acknowledgments

This project was supported by the National Key Project for Basic Research (2012CB417004).

Appendix A. Supplementary data

Supplementary data related to this article can be found at http://dx.doi.org/10.1016/j.envpol.2016.05.053.

References

Amirbahman, A., Pearce, A.R., Bouchard, R.J., Norton, S.A., Kahl, J.S., 2003. Relationship between hypolimnetic phosphorus and iron release from eleven lakes in Maine, USA. Biogeochemistry 65, 369–386.
Boers, P.C.M., Van Hese, O., 1988. Phosphorus release from the peaty sediments of the Loosdrecht Lakes (The Netherlands). Water Res. 22, 355–363.
Boström, B., Andersen, J.M., Fleischer, S., Jansson, M., 1988. Exchange of phosphorus across the sediment-water interface. Hydrobiologia 170, 229–244.
Cermelj, B., Bertuzzi, A., Faganeli, J., 1997. Modelling of pore water nutrient distribution and benthic fluxes in shallow coastal waters (Gulf of Trieste, Northern Adriatic). Water Air Soil Poll. 99, 435–443.
Chen, M.S., Ding, S.M., Liu, L., Xu, D., Han, C., Zhang, C.S., 2015. Iron-coupled inactivation of phosphorus in sediments by macrozoobenthos (chironomid larvae) bioturbation: evidences from high-resolution dynamic measurements. Environ. Pollut. 204, 241–247.
Christophoridis, C., Fytianos, K., 2006. Conditions affecting the release of phosphorus from surface lake sediments. J. Environ. Qual. 35, 1181–1192.
Correll, D.L., 1998. The role of phosphorus in the eutrophication of receiving waters: a review. J. Environ. Qual. 27, 261–266.
Ding, S.M., Han, C., Wang, Y.P., Yao, L., Wang, Y., Xu, D., Sun, Q., Williams, P.N., Zhang, C.S., 2015. In situ, high-resolution imaging of labile phosphorus in sediments of a large eutrophic lake. Water Res. 74, 100–109.
Ding, S.M., Jia, F., Xu, D., Sun, Q., Zhang, L., Fan, C.X., Zhang, C.S., 2011. High-resolution, two-dimensional measurement of dissolved reactive phosphorus in sediments using the diffusive gradients in thin films technique in combination with a routine procedure. Environ. Sci. Technol. 45, 9680–9686.
Ding, S.M., Sun, Q., Xu, D., Jia, F., He, X., Zhang, C.S., 2012. High-resolution simultaneous measurements of dissolved reactive phosphorus and dissolved sulfide: the first observation of their simultaneous release in sediments. Environ. Sci. Technol. 46, 8297–8304.
Ding, S.M., Wang, Y., Xu, D., Zhu, C.G., Zhang, C.S., 2013. Gel-based coloration technique for the submillimeter-scale imaging of labile phosphorus in sediments and soils with diffusive gradients in thin films. Environ. Sci. Technol. 47, 7821–7829.
Ding, S.M., Wang, Y., Wang, D., Li, Y.Y., Gong, M.D., Zhang, C.S., 2016. In situ, high-resolution evidence for iron-coupled mobilization of phosphorus in sediments. Sci. Rep. 6, 24341.
Einsele, W., 1936. Über die Beziehungen des Eisenkreislaufs zum Phosphatkreislauf im eutrophen See. Arch. Hydrobiol. 29, 664–686.
Fan, C.X., Zhang, L., Yang, L.Y., Huang, W.Y., Xu, P.Z., 2002. Simulation of internal loadings of nitrogen and phosphorus in a lake. Oceanol. Limnol. Sin. 33, 370–378.
Funes, A., de Vicente, J., Cruz-Pizarro, L., Álvarez-Manzaneda, I., de Vicente, I., 2016. Magnetic microparticles as a new tool for lake restoration: a microcosm experiment for evaluating the impact on phosphorus fluxes and sedimentary phosphorus pools. Water Res. 89, 366–374.
Golterman, H.L., 1988. The calcium-and iron bound phosphate phase diagram. Hydrobiologia 159, 149–151.
Golterman, H.L., 1995. The labyrinth of nutrient cycles and buffers in wetlands: results based on research in the Camargue (southern France). Hydrobiologia 315, 39–58.
Golterman, H.L., 1977. Sediments as a source of phosphate for algal growth. In: Interactions between Sediments and Fresh Water; Proceedings of an International Symposium, pp. 286–293.
Golterman, H.L., 2001. Phosphate release from anoxic sediments or 'What did Mortimer really write?'. Hydrobiologia 450, 99–106.
Hansen, K., Mouridsen, S., Kristensen, E., 1997. The impact of Chironomus plumosus larvae on organic matter decay and nutrient (N, P) exchange in a shallow eutrophic lake sediment following a phytoplankton sedimentation. Hydrobiologia 364, 65–74.
House, W.A., Casey, H., Donaldson, L., Smith, S., 1986. Factors affecting the coprecipitation of inorganic phosphate with calcite in hardwaters – I Laboratory studies. Water Res. 20, 917–922.
Hupfer, M., Gloess, S., Grossart, H.P., 2007. Polyphosphate-accumulating microorganisms in aquatic sediments. Aquat. Microb. Ecol. 47, 299.
Hupfer, M., Gtichter, R., Ruegger, R.R., 1995. Polyphosphate in lake sediments: 31P NMR spectroscopy as a tool for its identification. Limnol. Oceanogr. 40, 610–617.
Hupfer, M., Zak, D., Roβberg, R., Herzog, C., Pöthig, R., 2009. Evaluation of a well-established sequential phosphorus fractionation technique for use in calcite-rich lake sediments: identification and prevention of artifacts due to apatite formation. Limnol. Oceanogr. Methods 7, 399–410.
Jan, J., Borovec, J., Kopáček, J., Hejzlar, J., 2013. What do results of common sequential fractionation and single-step extractions tell us about P binding with Fe and Al compounds in non-calcareous sediments? Water Res. 47, 547–557.
Jensen, H.S., Andersen, F.Ø., 1992. Importance of temperature, nitrate, and pH for phosphate release from aerobic sediments of four shallow, eutrophic lakes. Limnol. Oceanogr. 37, 577–589.
Jensen, H.S., Kristensen, P., Jeppesen, E., Skytthe, A., 1992. Iron: phosphorus ratio in surface sediment as an indicator of phosphate release from aerobic sediments in shallow lakes. Hydrobiologia 235, 731–743.
Jensen, H.S., Mortensen, P.B., Andersen, F.Ø., Rasmussen, E., Jensen, A., 1995. Phosphorus cycling in a coastal marine sediment, Aarhus Bay. Den. Limnol. Oceanogr. 40, 908–917.
Jin, X.C., Tu, Q.Y., 1990. Lake eutrophication Survey Specification, second ed. China Environmental Science Press, p. 547.
Knuuttila, S., Pietiläinen, O.P., Kauppi, L., 1994. Nutrient balances and phytoplankton dynamics in two agriculturally loaded shallow lakes. Hydrobiologia 275, 359–369.
Kraal, P., Burton, E.D., Rose, A.L., Kocar, B.D., Lockhart, R.S., Grice, K., Bush, R.T., Tan, E., Webb, S.M., 2015. Sedimentary iron-phosphorus cycling under contrasting redox conditions in a eutrophic estuary. Chem. Geol. 392, 19–31.
Lewandowski, J., Hupfer, M., 2005. Effect of macrozoobenthos on two-dimensional small-scale heterogeneity of pore water phosphorus concentrations in lake sediments: a laboratory study. Limnol. Oceanogr. 50, 1106–1118.
Lewandowski, J., Laskov, C., Hupfer, M., 2007. The relationship between Chironomus plumosus burrows and the spatial distribution of porewater phosphate, iron and ammonium in lake sediments. Freshw. Biol. 52, 331–343.
Li, D.P., Huang, Y., 2010. Sedimentary phosphorus fractions and bioavailability as influenced by repeated sediment resuspension. Ecol. Eng. 36, 958–962.
Li, Y.H., Gregory, S., 1974. Diffusion of ions in seawater and in deepsea sediments. Geochim. Cosmochim. Acta 38, 703–714.
Liang, T., Ding, S.M., Zhang, C.S., Zhang, Z.L., Yan, J.C., Li, H.T., 2005. Fractionation of rare earth elements in plants 1, fractionation patterns and their forming mechanisms in different organs of Triticum aestivum. J. Rare Earth 23, 224–226.
Liu, C., Shao, S.G., Shen, Q.S., Fan, C.X., Zhang, L., Zhou, Q.l., 2016. Effects of riverine suspended particulate matter on the post-dredging increase in internal phosphorus loading across the sediment-water interface. Environ. Pollut. 211, 165–172.
Manheim, F.T., Waterman, L.S., 1974. Diffusimetry (diffusion constant estimation) on sediment cores by resistivity probe. Initial Rep. Deep-Sea Drill. Proj. 22, 663–670.
Mayer, T., Ptacek, C., Zanini, L., 1999. Sediments as a source of nutrients to hypereutrophic marshes of Point Pelee, Ontario, Canada. Water Res. 33, 1460–1470.
McCall, P.L., Tevesz, M.J., 1982. The effects of benthos on physical properties of freshwater sediments. In: Animal-sediment Relations. Springer, US, pp. 105–176.
Mejia, J., Roden, E.E., Ginder-Vogel, M.A., 2016. Influence of oxygen and nitrate on Fe (hydr) oxide mineral transformation and soil microbial communities during redox cycling. Environ. Sci. Technol. 50, 3580–3588.
Monbet, P., McKelvie, I.D., Worsfold, P.J., 2008. Combined gel probes for the in situ determination of dissolved reactive phosphorus in porewaters and characterization of sediment reactivity. Environ. Sci. Technol. 42, 5112–5117.
Mortimer, C.H., 1941. The exchange of dissolved substances between mud and water in lakes. J. Ecol. 29, 280–329.
Murphy, J., Riley, J., 1962. A modified single solution method for the determination of phosphate in natural waters. Anal. Chim. Acta 27, 31–36.
Murray, G.C., Hesterberg, D., 2006. Iron and phosphate dissolution during abiotic reduction of ferrihydrite-boehmite mixtures. Soil Sci. Soc. Am. J. 70, 1318–1327.
Olsen, S., 1964. Phosphate equilibrium between reduced sediments and water, laboratory experiments with radioactive phosphorus. Verh. Int. Ver. Limnol. 13, 915–922.
Panther, J.G., Teasdale, P.R., Bennett, W.W., Welsh, D.T., Zhao, H.J., 2011. Comparing dissolved reactive phosphorus measured by DGT with ferrihydrite and titanium dioxide adsorbents: anionic interferences, adsorbent capacity and deployment time. Anal. Chim. Acta 698, 20–26.
Penn, M.R., Auer, T., Van Orman, E.L., Korienek, J.J., 1995. Phosphorus diagenesis in

lake sediments: investigations using fractionation techniques. Mar. Freshw. Res. 46, 89–99.
Petticrew, E.L., Arocena, J.M., 2001. Evaluation of iron-phosphate as a source of internal lake phosphorus loadings. Sci. Total Environ. 266, 87–93.
Pichette, C., Zhang, H., Sauvé, S., 2009. Using diffusive gradients in thin-films for in situ monitoring of dissolved phosphate emissions from freshwater aquaculture. Aquaculture 286, 198–202.
Pitkänen, H., Lehtoranta, J., Räike, A., 2001. Internal nutrient fluxes counteract decreases in external load: the case of the estuarial eastern Gulf of Finland, Baltic Sea. Ambio 30, 195–201.
Psenner, R., Pucsko, R., 1988. Phosphorus fractionation: advantages and limits of the method for the study of sediment P origins and interactions. Arch. Hydrobiol. Beih. Ergebn. Limnol. 30, 43–59.
Reitzel, K., Hansen, J., Andersen, F.Ø., Hansen, K.S., Jensen, H.S., 2005. Lake restoration by dosing aluminum relative to mobile phosphorus in the sediment. Environ. Sci. Technol. 39, 4134–4140.
Roden, E.E., Zachara, J.M., 1996. Microbial reduction of crystalline iron (III) oxides: influence of oxide surface area and potential for cell growth. Environ. Sci. Technol. 30, 1618–1628.
Rodriguez, J.B., Self, J.R., Soltanpour, P.N., 1994. Optimal conditions for phosphorus analysis by the ascorbic acid-molybdenum blue method. Soil Sci. Soc. Am. J. 58, 866–870.
Rydin, E., 2000. Potentially mobile phosphorus in Lake Erken sediment. Water Res. 34, 2037–2042.
Scally, S., Davison, W., Zhang, H., 2006. Diffusion coefficients of metals and metal complexes in hydrogels used in diffusive gradients in thin films. Anal. Chim. Acta 558, 222–229.
Schindler, D.W., 2006. Recent advances in the understanding and management of eutrophication. Limnol. Oceanogr. 51, 356–363.
Schoepfer, S.D., Shen, J., Wei, H.Y., Tyson, R.V., Ingall, E., Algeo, T.J., 2015. Total organic carbon, organic phosphorus, and biogenic barium fluxes as proxies for paleomarine productivity. Earth Sci. Rev. 149, 23–52.
Smith, V.H., Schindler, D.W., 2009. Eutrophication science: where do we go from here? Trends Ecol. Evol. 24, 201–207.
Søndergaard, M., Jensen, J.P., Jeppesen, E., 2003. Role of sediment and internal loading of phosphorus in shallow lakes. Hydrobiologia 506, 135–145.
Søndergaard, M., Kristensen, P., Jeppesen, E., 1992. Phosphorus release from resuspended sediment in the shallow and wind-exposed Lake Arresø, Denmark. Hydrobiologia 228, 91–99.
Spagnoli, F., Bergamini, M.C., 1997. Water-sediment exchange of nutrients during early diagenesis and resuspension of anoxic sediments from the Northern Adriatic Sea shelf. Water Air Soil Poll. 99, 541–556.
Stephen, D., Moss, B., Phillips, G., 1997. Do rooted macrophytes increase sediment phosphorus release? Hydrobiologia 342, 27–34.
Suzumura, M., Kamatani, A., 1995. Mineralization of inositol hexaphosphate in aerobic and anaerobic marine sediments: implications for the phosphorus cycle. Geochim. Cosmochim. Acta 59, 1021–1026.
Tamura, H., Goto, K., Yotsuyanagi, T., Nagayama, M., 1974. Spectrophotometric determination of iron (II) with 1, 10-phenanthroline in the presence of large amounts of iron (III). Talanta 21, 314–318.
Tang, X.Q., Wu, M., Li, Q.Y., Lin, L., Zhao, W.H., 2014. Impacts of water level regulation on sediment physic-chemical properties and phosphorus adsorption-desorption behaviors. Ecol. Eng. 70, 450–458.
Ullman, W.J., Aller, R.C., 1982. Diffusion coefficients in nearshore marine sediments. Limnol. Oceanogr. 27, 552–556.
Wang, L.Q., Liang, T., Kleinman, P.J., Cao, H.Y., 2011. An experimental study on using rare earth elements to trace phosphorous losses from nonpoint sources. Chemosphere 85, 1075–1079.
Wang, Y., Jiang, X., Li, Y.F., Wang, S.H., Wang, W.W., Cheng, G.L., 2014. Spatial and temporal distribution of nitrogen and phosphorus and nutritional characteristics of water in Dongting Lake. Res. Environ. Sci. 27, 484–491.
Watts, C.J., 2000. The effect of organic matter on sedimentary phosphorus release in an Australian reservoir. Hydrobiologia 431, 13–25.
Widerlund, A., Davison, W., 2007. Size and density distribution of sulfide-producing microniches in lake sediments. Environ. Sci. Technol. 41, 8044–8049.
Wu, D., Hua, Z.L., 2014. The effect of vegetation on sediment resuspension and phosphorus release under hydrodynamic disturbance in shallow lakes. Ecol. Eng. 69, 55–62.
Xu, D., Chen, Y.F., Ding, S.M., Sun, Q., Wang, Y., Zhang, C.S., 2013. Diffusive gradients in thin films technique equipped with a mixed binding gel for simultaneous measurements of dissolved reactive phosphorus and dissolved iron. Environ. Sci. Technol. 47, 10477–10484.
Xu, D., Wu, W., Ding, S.M., Sun, Q., Zhang, C.S., 2012. A high-resolution dialysis technique for rapid determination of dissolved reactive phosphate and ferrous iron in pore water of sediments. Sci. Total. Environ. 421, 245–252.
Xu, W.L., Wang, X.R., Xian, Q.M., Luo, J., Liu, Z.M., Geng, J.J., 2011. Assessment of the influence of P availability of sediments in Lake Taihu to Microcystis aeruginosa using different methods. China Environ. Sci. 31, 1486–1491.
You, B.S., Zhong, J.C., Fan, C.X., Wang, T.C., Zhang, L., Ding, S.M., 2007. Effects of hydrodynamics processes on phosphorus fluxes from sediment in large, shallow Taihu Lake. J. Environ. Sci. 19, 1055–1060.
Zhang, C.S., Ding, S.M., Xu, D., Tang, Y., Wong, M.H., 2014. Bioavailability assessment of phosphorus and metals in soils and sediments: a review of diffusive gradients in thin films (DGT). Environ. Monit. Assess. 186, 7367–7378.
Zhang, H., Davison, W., 1995. Performance characteristics of diffusion gradients in thin films for the in situ measurement of trace metals in aqueous solution. Anal. Chem. 67, 3391–3400.
Zhang, L., Fan, C.X., Wang, J.J., Zheng, C.H., 2006. Space-time dependent variances of ammonia and phosphorus flux on sediment water interface in Lake Taihu. Environ. Sci. 27, 1537–1543.

Please cite this article in press as: Gao, Y., et al., High-resolution imaging of labile phosphorus and its relationship with iron redox state in lake sediments, Environmental Pollution (2016), http://dx.doi.org/10.1016/j.envpol.2016.05.053